

# CrystEngComm

Accepted Manuscript

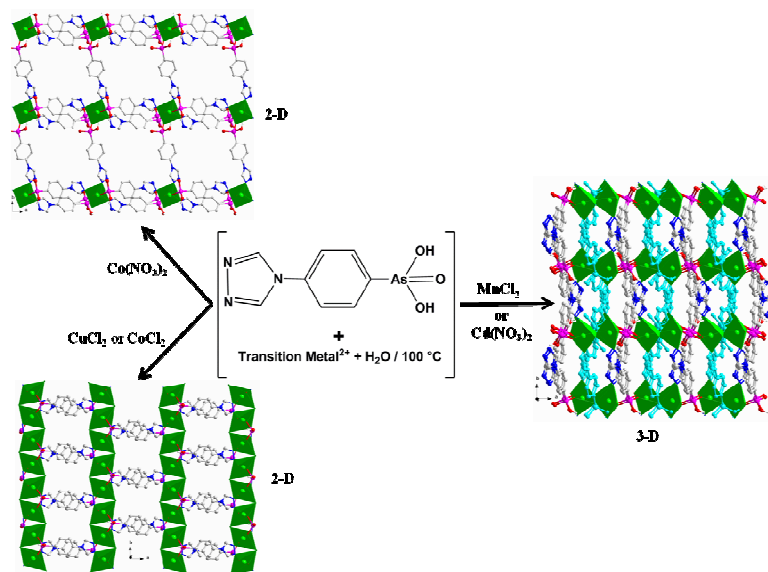


This is an *Accepted Manuscript*, which has been through the Royal Society of Chemistry peer review process and has been accepted for publication.

*Accepted Manuscripts* are published online shortly after acceptance, before technical editing, formatting and proof reading. Using this free service, authors can make their results available to the community, in citable form, before we publish the edited article. We will replace this *Accepted Manuscript* with the edited and formatted *Advance Article* as soon as it is available.

You can find more information about *Accepted Manuscripts* in the [Information for Authors](#).

Please note that technical editing may introduce minor changes to the text and/or graphics, which may alter content. The journal's standard [Terms & Conditions](#) and the [Ethical guidelines](#) still apply. In no event shall the Royal Society of Chemistry be held responsible for any errors or omissions in this *Accepted Manuscript* or any consequences arising from the use of any information it contains.



Five coordination polymers were prepared using the hydrothermal/sovothermal reactions of transition metal salts (Co<sup>2+</sup>, Cu<sup>2+</sup>, Mn<sup>2+</sup> and Cd<sup>2+</sup>) and a newly synthesized bifunctional arsonic acid ligand that contains an auxiliary triazole group. Their crystal structures, luminescent and magnetic properties are reported.

# Exploring the Coordination Chemistry of Bifunctional Organoarsonate Ligands: Syntheses and Characterisation of Coordination Polymers that Contain 4-(1,2,4-triazol-4-yl)phenylarsonic Acid

Jian-Di Lin,<sup>a</sup> Rodolphe Clérac,<sup>b,c</sup> Mathieu Rouzières,<sup>b,c</sup> Munuswamy Venkatesan,<sup>d</sup> Theresa O. Chimamkam,<sup>a</sup> Wolfgang Schmitt<sup>\*,a</sup>

<sup>a</sup> School of Chemistry & CRANN, University of Dublin, Trinity College, Dublin 2, Ireland.

E-mail: schmittw@tcd.ie; Fax: +353 1 671 2826; Tel: +353 1 896 3495.

<sup>b</sup> CNRS, CRPP, UPR 8641, F-33600 Pessac, France.

<sup>c</sup> Univ. Bordeaux, CRPP, UPR 8641, F-33600 Pessac, France.

<sup>d</sup> School of Physics & CRANN, University of Dublin, Trinity College, Dublin 2, Ireland.

## Abstract

This account describes the coordination chemistry of a novel bifunctional arsonic acid ligand, 4-(1,2,4-triazol-4-yl)phenylarsonic acid (H<sub>2</sub>TPAA) that contains a triazole group. Hydrothermal reactions of transition metal salts with H<sub>2</sub>TPAA produced five unprecedented coordination polymers: [Co(H<sub>2</sub>TPAA)(HTPAA)<sub>2</sub>·H<sub>2</sub>O (**1**), M(HTPAA)Cl·2H<sub>2</sub>O (M = Cu (**2**), Co (**3**)) and M(HTPAA)<sub>2</sub> (M = Mn (**4**), Cd (**5**)). These five polymers have been fully characterized by single crystal and powder X-ray diffraction, thermogravimetric analysis, infra-red spectroscopy and elemental analysis. Single crystal X-ray diffraction reveals that **1**, **2** and **3** adopt 2-D layered structural motifs whereas **4** and **5** are 3-D frameworks. **1** and **3** are the first examples of arsonate-stabilised cobalt(II) coordination polymers. Likewise, **4** is recognised as the first record of a Mn<sup>II</sup> arsonate coordination polymer with 3-D framework topology. Its isostructural Cd analogue **5** shows characteristic ligand-centered fluorescence properties. Magnetic measurements of **2** and **4** reveal predominant antiferromagnetic interactions between their respective spin centers while, in agreement with its chain structure, **3** exhibits one-dimensional magnetic behavior with weak ferromagnetic interactions between the spin centres.

## Introduction

Over recent years, there has been a significant interest in the design and synthesis of metal phosphonates due to their potential applications in electro-optical devices, in catalysis, sensors or as ion-exchange materials.<sup>1-2</sup> Several synthetic strategies have been explored to prepare and isolate crystalline metal phosphonates with diverse structural and electronic attributes. The applied synthetic methodologies include the attachment of functional auxiliary groups (crown ether, amine, hydroxyl, or/and carboxylate, etc) to the phosphonic acid backbone thus introducing a second potential linker to increase the dimensionality of the resulting frameworks or tune their properties.<sup>3</sup> However, to date, most of the reported extended metal phosphonates display layered structures in which the metal centers are bridged by the phosphonate groups. One-dimensional (1-D) and porous three-dimensional (3-D) networks have rarely been reported.<sup>4</sup> Very recently, a ligand that combines a triazole moiety with a phosphonate functionality, 4-(1, 2, 4-triazol-4-yl)phenylphosphonic acid (H<sub>2</sub>ptz) has been exploited to prepare three two-dimensional (2-D) coordination polymers containing Ni(II), Co(II) or Mn(II) metal ions.<sup>5</sup>

Metal arsonates are expected to show structural attributes that are similar to those of the metal phosphonates. However, the larger ionic radius of As(V) compared to that of P(V) can be expected to result in different molecular architectures and physical properties. Most of the reported metal organoarsonates are hybrid polyoxometalate (POM) clusters based on V, Mo or W.<sup>6</sup> In particular, Zubieta extensively explored the formation of such hybrid POMs.<sup>6a, b, 6d, 6m, n</sup> Recently, we reported several capsular arsonate-stabilised polyoxovanadates that incorporate substituted phenylarsonate and investigated their 3-D assembly.<sup>7</sup> In such POMs, each arsonate functionality bridges several metal centers and shows a coordination behaviour that is closely comparable to that of the corresponding phosphonate-stabilised POMs.<sup>3h, 7</sup> Ma *et al.* have reported several tin oxo-complexes that contain organoarsonates and which were isolated by solvothermal techniques.<sup>8</sup> Synthetic approaches to Pd-based arsonate complexes were also explored under the hydrothermal conditions.<sup>9</sup> Recently, Sun *et al.* reported the first examples of uranyl arsonates that employ phenylarsonic acid as stabilising ligand.<sup>10</sup> To date, arsonate-stabilised transition metal (TM) coordination polymers are significantly less developed and investigated compared to the corresponding phosphonate compounds. A CCDC search reveals that arsonate-stabilised TM coordination polymers mainly adopt 1-D and 2-D structures<sup>11</sup> while corresponding 3-D structures are rather rare. Remarkable

examples of the latter are a Zn(II)-based framework with *crb* topology, Zn(4-apa) (4-apaH<sub>2</sub> = 4-aminophenylarsonic acid)<sup>12</sup> and a Cd(II)-based framework, Cd(H<sub>2</sub>L)<sub>2</sub>·2H<sub>2</sub>O (H<sub>3</sub>L = 2-(4-arsenophenylamino)acetic acid).<sup>13</sup> Other relevant 3-D metal coordination polymers that incorporate mixed organoarsenate and carboxylate ligands are two lead-based and three isostructural lanthanide-based compounds: Pb<sub>5</sub>(SIP)<sub>2</sub>(L1)<sub>2</sub>(H<sub>2</sub>O), Pb<sub>3</sub>(SIP)(L2)(H<sub>2</sub>O)<sup>14</sup> and Ln<sub>2</sub>(HL2)<sub>2</sub>(C<sub>2</sub>O<sub>4</sub>)(H<sub>2</sub>O)<sub>2</sub> (Ln = Nd, Sm or Eu, H<sub>2</sub>L1 = phenylarsonic acid, H<sub>3</sub>L2 = 4-hydroxy-3-nitrophenylarsonic acid and NaH<sub>2</sub>SIP = 5-sulfoisophthalic acid monosodium salt).<sup>15</sup> In order to explore the synthesis of arsonate-based coordination polymers with 3-D framework topology, we successfully synthesized a novel bifunctional ligand 4-(1,2,4-triazol-4-yl)phenylarsonic acid (H<sub>2</sub>TPAA) that relates to the previously mentioned phosphonate ligand, H<sub>2</sub>ptz. The preparation of the extended coordination polymers was carried out under hydrothermal conditions. Our synthetic approach led to a series of transition metal coordination polymers, [Co(H<sub>2</sub>TPAA)(HTPAA)<sub>2</sub>]·H<sub>2</sub>O (**1**), M(HTPAA)Cl·2H<sub>2</sub>O (M = Cu (**2**) and Co (**3**)), M(HTPAA)<sub>2</sub> (M = Mn (**4**) and Cd (**5**)). Among these five coordination polymers, **1**, **2** and **3** adopt 2-D layered structures whilst **4** and **5** are 3-D frameworks. Herein, we report their syntheses, crystal structures, luminescent and magnetic properties.

## 2. Experimental section

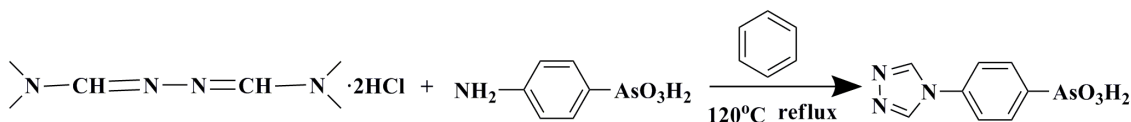
### 2.1 Materials and Instrumentation.

The novel H<sub>2</sub>TPAA ligand, 4-(1,2,4-triazol-4-yl)phenylarsonic acid, was synthesized from *N,N*-dimethylformamide azine dihydrochloride using a general literature procedure.<sup>16</sup> All reagents were purchased from Sigma-Aldrich and used as received without further purification. <sup>1</sup>H and <sup>13</sup>C nuclear magnetic resonance (NMR) data were recorded on a Bruker DPX 400 spectrometer (400.13 MHz for <sup>1</sup>H, 100.63 MHz for <sup>13</sup>C). Fourier transform infrared spectroscopy (FTIR) data were collected on a Perkin-Elmer Spectrum one FT-IR Spectrometer. Thermogravimetric analysis (TGA) was performed under an air atmosphere on a Perkin-Elmer Pyrus 1 TGA from 30-800 °C at a heating rate of 10 °C/min. Powder X-ray diffraction (PXRD) data were recorded on a Siemens D500 X-ray diffractometer at 40 kV, 30 mA using Cu-K $\alpha$  radiation ( $\lambda = 1.54056 \text{ \AA}$ ), with a scan speed of 3°/min and a step size of 0.05° in 2 $\theta$  at room temperature. The simulated patterns were derived from the programme Mercury Version 1.4 software. Elemental analyses (C, H, and N) were obtained from the Microanalysis Laboratory, School of Chemistry and Chemical Biology, University College Dublin. The magnetic susceptibility measurements of **2**, **3** and **4** were obtained with the use

of MPMS-XL Quantum Design SQUID magnetometer. Measurements were performed on polycrystalline samples of 20.3, 18.87 and 8.5 mg for **2**, **3** and **4** respectively, which were measured in polyethylene bags ( $3 \times 0.5 \times 0.02$  cm); ac susceptibility measurements for **3** were recorded using an oscillating ac field of 3 Oe with frequency of 1000 Hz.  $M$  vs  $H$  measurements at 100 K at different magnetic fields were performed to confirm the absence of potential ferromagnetic impurities. The magnetic data were corrected for the sample holder and the diamagnetic contributions. Solid state fluorescence measurements were carried out using Fluorolog®-3 Spectrofluorometer.

## 2.2 Synthesis of 4-(1,2,4-triazol-4-yl)phenylarsonic acid (H<sub>2</sub>TPAA)

250 mL of benzene was added to a mixture of *N,N*-dimethylformamide azine dihydrochloride (17.21 g, 80 mmol) and 4-aminophenylarsonic acid (17.36 g, 80 mmol) and the resulting turbid solution was refluxed at 120 °C for three days. Afterwards, the the solvent was decanted off, 100 mL ethanol was added and the mixture was stirred for ten minutes. The formed solid product was collected by filtration and washed with ethanol until the filtrate became colorless. The product was purified by recrystallization from boiling water. Thin plate crystals were obtained after cooling and were filtered off and dried at room temperature (Scheme 1, yield: 6.57 g, 30.5 % based on 4-aminophenylarsonic acid). IR ( $\bar{\nu}/\text{cm}^{-1}$ ): 3134 (vw), 2985 (vw), 2677 (vw), 2281 (w), 1700 (w), 1597 (w), 1528 (w), 1417 (vw), 1380 (vw), 1330 (w), 1268 (vw), 1229 (vw), 1103 (w), 1040 (vw), 990 (vw), 932 (s), 850 (w), 825 (s), 747 (vs), 722 (s), 668 (w). <sup>1</sup>H NMR (DMSO-d<sub>6</sub>),  $\delta$ : 9.25 (2H, s, triazole), 7.97 (2H, m, phenyl) and 7.94 (2H, m, phenyl) (ESI, Fig. S9). <sup>13</sup>C NMR (DMSO-d<sub>6</sub>),  $\delta$ : 141.3, 137.3, 133.3, 131.9, 121.8 (ESI, Fig. S10).



Scheme 1. Synthetic route to H<sub>2</sub>TPAA

## 2.3 Syntheses of the transition metal complexes

[Co(H<sub>2</sub>TPAA)(HTPAA)<sub>2</sub>]·H<sub>2</sub>O (**1**) Co(NO<sub>3</sub>)<sub>2</sub>·6H<sub>2</sub>O (0.2 mmol), H<sub>2</sub>TPAA (0.1 mmol) and 4 mL of H<sub>2</sub>O were added into a 10 mL reaction vial and sealed. The mixture was heated to 100 °C and kept at this temperature for one day. Pink columnar crystals of **1** were obtained and washed with H<sub>2</sub>O before drying in air at room temperature (yield: 25 mg, 85% based on

H<sub>2</sub>TPAA). Elemental analysis (%): calcd. for C<sub>24</sub>H<sub>24</sub>As<sub>3</sub>CoN<sub>9</sub>O<sub>10</sub>, C 32.68 H 2.74 N 14.29; Found C 32.82 H 2.51 N 14.53. IR ( $\bar{\nu}/\text{cm}^{-1}$ ): 3120 (vw), 1738 (vw), 1599 (w), 1531 (s), 1418 (vw), 1372 (vw), 1324 (vw), 1250 (m), 1103 (s), 1028 (w), 1014 (w), 978 (vw), 859 (s), 825 (s), 764 (m), 726 (m), 705 (m).

**Cu(HTPAA)Cl·2H<sub>2</sub>O (2)** CuCl<sub>2</sub>·2H<sub>2</sub>O (0.2 mmol), H<sub>2</sub>TPAA (0.1 mmol), 0.1 mL of 36.5% HCl<sub>aq</sub>. and 5 mL of H<sub>2</sub>O were added into a 20 mL Teflon-lined stainless steel autoclave. The mixture was heated to 100 °C and kept at this temperature for two days before it was allowed to cool to room temperature. The resulting pale blue solution was left to evaporate at room temperature producing pale blue needle crystals of **2**, which were washed thoroughly with H<sub>2</sub>O, and dried in air at room temperature (yield: 25 mg, 62% based on H<sub>2</sub>TPAA). Elemental analysis (%): calcd. for C<sub>8</sub>H<sub>11</sub>AsClCuN<sub>3</sub>O<sub>5</sub>, C 23.84 H 2.75 N 10.42; Found C 23.90 H 2.46 N 10.59. IR ( $\bar{\nu}/\text{cm}^{-1}$ ): 3409 (w), 3143 (w), 2394 (w), 1640 (w), 1597 (w), 1549 (m), 1425 (vw), 1338 (w), 1305 (vw), 1253 (m), 1226 (m), 1110 (m), 1064 (m), 1019 (vw), 981 (w), 846 (s), 832 (s), 774 (s), 722 (m), 707 (m).

**Co(HTPAA)Cl·2H<sub>2</sub>O (3)** CoCl<sub>2</sub>·6H<sub>2</sub>O (0.2 mmol), H<sub>2</sub>TPAA (0.1 mmol), 0.1 mL of 36.5% HCl<sub>aq</sub>, 1 mL of DMF and 5 mL of H<sub>2</sub>O were placed in a 20 mL Teflon-lined stainless steel. The mixture was heated to 100 °C and kept at this temperature for two days and cooled to room temperature in one day. Violet prism crystals **3** were collected, washed thoroughly with H<sub>2</sub>O, and dried in air at room temperature (yield: 30 mg, 75% based on H<sub>2</sub>TPAA). DMF is necessary for the crystallisation of the compound; if the reaction of CoCl<sub>2</sub>·6H<sub>2</sub>O and H<sub>2</sub>TPAA is carried out in pure H<sub>2</sub>O at 100 °C, **1** is reproducibly obtained. Elemental analysis (%): calcd. for C<sub>8</sub>H<sub>11</sub>AsClCoN<sub>3</sub>O<sub>5</sub>, C 24.11 H 2.78 N 10.54; Found C 24.23 H 2.51 N 10.62. IR ( $\bar{\nu}/\text{cm}^{-1}$ ): 3543 (w), 3225 (w), 3133 (w), 2393 (w), 1646 (w), 1600 (w), 1546 (m), 1421 (w), 1385 (vw), 1332 (w), 1300 (w), 1251 (m), 1108 (m), 1053 (m), 1020 (vw), 999 (vw), 981 (w), 853 (s), 829 (s), 762 (s), 725 (w), 676 (vw).

**Mn(HTPAA)<sub>2</sub> (4)** MnCl<sub>2</sub>·4H<sub>2</sub>O (0.2 mmol), H<sub>2</sub>TPAA (0.1 mmol), 4,4'-bipyridine (0.1 mmol) and 4 mL of H<sub>2</sub>O were added into a 10 mL reaction vial and sealed. The mixture was heated to 100 °C and kept at this temperature for two days before it was allowed to cool to room temperature. Colourless needle-like crystals of **4** were obtained, filtered off and washed thoroughly with H<sub>2</sub>O and dried in air at room temperature (yield: 18 mg, 30% based on H<sub>2</sub>TPAA). Although 4,4'-bipyridine was not incorporated into this compound, its absence in

the reaction mixture gives rise to lower yield of the product. Elemental analysis (%): calcd. For  $C_{16}H_{14}As_2MnN_6O_6$ , C 32.51 H 2.39 N 14.22, Found, C 32.61 H 2.55 N 14.31. IR ( $\bar{\nu}/\text{cm}^{-1}$ ): 3127 (vw), 3114 (w), 3059 (vw), 2314 (w), 1681 (w), 1595 (m), 1538 (s), 1522 (s), 1418 (w), 1383 (w), 1365 (w), 1332 (w), 1289 (w), 1253 (w), 1239 (m), 1099 (m), 1083 (w), 1028 (w), 1013 (w), 1007 (w), 850 (w), 806 (s), 734 (s), 723 (s), 706 (w).

**Cd(HTPAA)<sub>2</sub> (5)**  $Cd(NO_3)_2 \cdot 4H_2O$  (0.2 mmol) and  $H_2TPAA$  (0.1 mmol) and 4 mL of  $H_2O$  were added into a 10 mL reaction vial and sealed. The mixture was heated to 100 °C and kept at this temperature for two days before it was allowed to cool to room temperature. Colourless needle-like crystals of **5** were obtained, filtered off, washed thoroughly with  $H_2O$  and dried in air at room temperature (yield: 30 mg, 46% based on  $H_2TPAA$ ). Elemental analysis (%): calcd. for  $C_{16}H_{14}As_2CdN_6O_6$ , C 29.63 H 2.18 N 12.96; Found C 29.51 H 2.31 N 12.85. IR ( $\bar{\nu}/\text{cm}^{-1}$ ): 3113 (w), 2259 (w), 1674 (w), 1596 (m), 1536 (s), 1524 (s), 1418 (w), 1381 (vw), 1367 (vw), 1331 (w), 1290 (w), 1241 (s), 1101 (s), 1084 (w), 1029 (w), 1015 (m), 938 (s), 814 (s), 723 (s), 706 (w).

## 2.4 X-Ray crystallography

The data collections of **1**, **4** and **5** were carried out using a Bruker Smart APEX CCD X-ray diffractometer at 200 K while those of **2** and **3** were carried out using a Rigaku 724 CCD X-ray diffractometer at 150 K, using graphite-monochromated Mo-K $\alpha$  radiation ( $\lambda = 0.71073$  Å). The data collection of  $H_2TPAA$  was carried out on a Bruker APEX Duo CCD X-ray diffractometer at 100 K using graphite-monochromated Mo-K $\alpha$  radiation ( $\lambda = 0.71073$  Å). The structures of the five coordination compounds and 4-(1,2,4-triazol-4-yl)phenylarsonic acid ( $H_2TPAA$ ) were solved by direct methods using SHELXS-97, integrated using the OLEX2 software<sup>17</sup> and refined using the SHELXL-97 programme.<sup>18</sup> All the non-hydrogen atoms were refined anisotropically. The hydrogen atoms of **1**, **2** and  $H_2TPAA$  were treated using a mixture of independent and constrained refinement parameters. The positions of the hydrogen atoms of the  $HTPAA^-$  anion in **2** and **3** were calculated; the H-atoms of the lattice water molecules in **2** and **3** were not refined. The H-positions of **4** and **5** were calculated and refined isotropically using fixed thermal factors. The  $AsO_3$  group in **1** exhibits a positional disorder over two sites ( $As1A$ ,  $O11$ ,  $O12$ ,  $O13$  and  $As1B$ ,  $O11$ ,  $O12'$ ,  $O13'$ ). The site occupancies of ( $As1A$ ,  $O12$ ,  $O13$ ) and ( $As1B$ ,  $O12'$ ,  $O13'$ ) in **1** are (0.83, 0.89, 0.86) and (0.17, 0.11, 0.14), respectively.  $O12'$  and  $O13'$  in **1** were refined isotropically. The hydrogen

atom (H13') of O13' in **1** was not included in the final refinement to avoid alerts that result from short H-H contacts that arise from the refinement of the positional disorder of the As1O<sub>3</sub> group. The benzene ring in H<sub>2</sub>TPAA also reveals a positional disorder over two sites (C3, C4, C5, C6, C7, C8 and C3, C4', C5', C6, C7', C8'). The site occupancies of (C4, C5, C7, C8) and (C4', C5', C7', C8') are (0.54, 0.54, 0.51, 0.51) and (0.46, 0.46, 0.49, 0.49), respectively. The As1–O1, As1–O2 and As1–O3 bond lengths in H<sub>2</sub>TPAA are 1.719(5), 1.721(5) and 1.627(5) Å, consequently O1 and O2 are assigned as hydroxyl oxygen atoms (ESI, Fig. S11). Details of X-ray analysis, including the crystal parameters, data collection and refinement parameters for compounds **1-5** are summarized in Table 1. Selected bond lengths, angles and hydrogen-bond interactions are given in the Tables S1.1 to S5.2 (ESI). Further details of the crystal structure determination have been deposited with the Cambridge Crystallographic Data Centre. CCDC No. for **1**, **2**, **4**, **5** and H<sub>2</sub>TPAA are: 958075–958079, and 974651 for **3**.

**Table 1** Crystal data and structure refinement information for H<sub>2</sub>TPAA and compounds **1-5**.

$${}^a R_I = \sum[|F_o| - |F_c|] / \sum|F_o|; {}^b wR_2 = [\sum w(F_o^2 - F_c^2)^2 / \sum w(F_o^2)^2]^{0.5}.$$

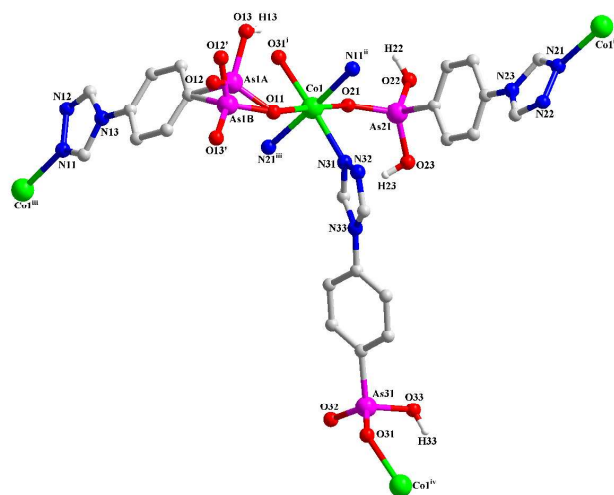
compound	H <sub>2</sub> TPAA	<b>1</b>	<b>2</b>	<b>3</b>	<b>4</b>	<b>5</b>
Empirical formula	C <sub>8</sub> H <sub>8</sub> AsN <sub>3</sub> O <sub>3</sub>	C <sub>24</sub> H <sub>24</sub> As <sub>3</sub> CoN <sub>9</sub> O <sub>9</sub> ·H <sub>2</sub> O	C <sub>8</sub> H <sub>7</sub> AsClCuN <sub>3</sub> O <sub>3</sub> ·2(H <sub>2</sub> O)	C <sub>8</sub> H <sub>7</sub> AsClCoN <sub>3</sub> O <sub>3</sub> ·2(H <sub>2</sub> O)	C <sub>16</sub> H <sub>14</sub> As <sub>2</sub> MnN <sub>6</sub> O <sub>6</sub>	C <sub>16</sub> H <sub>14</sub> As <sub>2</sub> CdN <sub>6</sub> O <sub>6</sub>
Formula weight	269.09	882.21	403.11	398.50	591.11	648.57
Crystal system	Monoclinic	Monoclinic	Monoclinic	Monoclinic	Monoclinic	Monoclinic
Space group	<i>P</i> 2 <sub>1</sub> / <i>c</i>	<i>P</i> 2 <sub>1</sub> / <i>n</i>	<i>C</i> 2/ <i>m</i>	<i>C</i> 2/ <i>m</i>	<i>P</i> 2 <sub>1</sub> / <i>c</i>	<i>P</i> 2 <sub>1</sub> / <i>c</i>
<i>a</i> , Å	6.0120(9)	11.019(2)	20.454(4)	20.875(4)	8.5378(17)	8.6818(5)
<i>b</i> , Å	21.594(3)	12.676(3)	7.7512(16)	7.6129(15)	17.151(3)	17.1961(9)
<i>c</i> , Å	8.9646(9)	21.167(4)	8.4433(17)	8.5776(17)	12.690(3)	12.8662(7)
β (°)	126.135(7)	98.13(3)	102.15(3)	101.41(3)	96.98(3)	96.906(1)
<i>V</i> (Å <sup>3</sup> )	939.9(2)	2927.0(10)	1308.7(5)	1336.2(5)	1844.5(6)	1906.90(18)
<i>Z</i>	4	4	4	4	4	4
Temperature (K)	100	200	150	150	200	200
μ (mm <sup>-1</sup> )	3.61	4.03	4.40	3.959	4.33	4.64
<i>D</i> <sub>calcd</sub> (g/cm <sup>3</sup> )	1.902	2.002	2.026	1.961	2.129	2.259
reflections collected	9217	17467	7137	4634	10927	11347
independent reflections	1738	5440	1254	1196	3423	3541
reflections [ <i>I</i> > 2σ( <i>I</i> )]	1710	4862	888	1188	3092	3342
<i>R</i> <sub>int</sub>	0.0266	0.0240	0.0393	0.0272	0.0281	0.0245
<i>R</i> <sub><i>I</i></sub> <sup><i>a</i></sup> , <i>wR</i> <sub>2</sub> <sup><i>b</i></sup> [ <i>I</i> > 2σ( <i>I</i> )]	0.0593, 0.1344	0.0259, 0.0737	0.0500, 0.1663	0.0365, 0.1015	0.0257, 0.0598	0.0206, 0.0513
<i>R</i> <sub><i>I</i></sub> <sup><i>a</i></sup> , <i>wR</i> <sub>2</sub> <sup><i>b</i></sup> (all data)	0.0601, 0.1348	0.0298, 0.0758	0.0601, 0.1736	0.0366, 0.1016	0.0296, 0.0615	0.0221, 0.0524
goodness-of-fit	1.068	1.055	0.999	1.075	1.037	1.029

### 3 Results and discussion

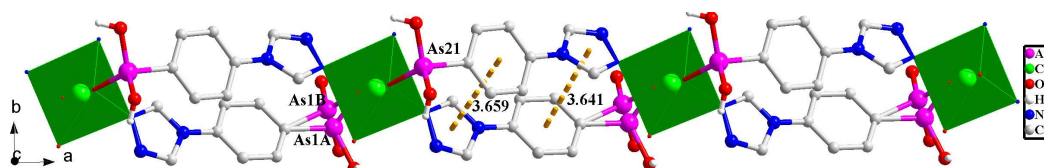
The compounds **1-5** were produced reproducibly in moderate yields under hydrothermal reaction conditions at a temperature of 100°C (*vide supra*). A structural rearrangement between the Co(II) compounds **2** and **3** is promoted by the presence of DMF as co-solvent. All compounds form under acidic conditions that are comparable to those applied for the formation of TM organophosphonate complexes. Elevated pH values generally resulted in microcrystalline or amorphous precipitates under the applied reaction conditions.

### 3.1 Structural description of the complexes

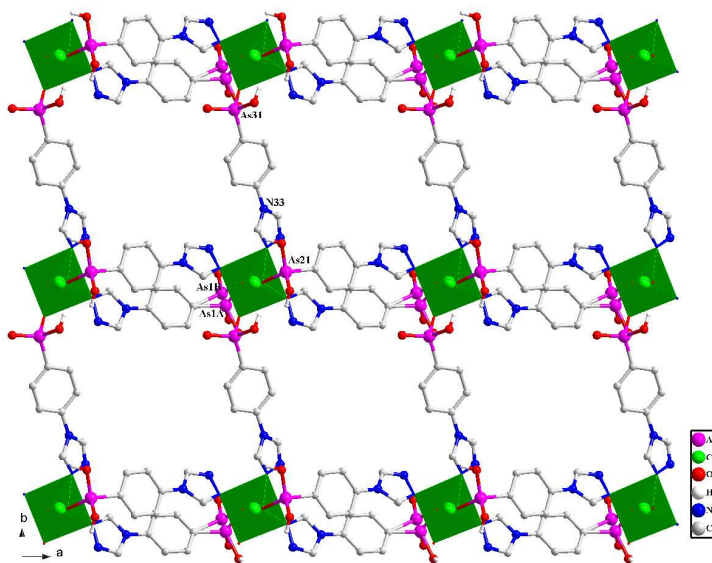
**[Co(H<sub>2</sub>TPAA)(HTPAA)<sub>2</sub>·H<sub>2</sub>O (1)]** Compound **1** crystallizes in the monoclinic space group *P*2<sub>1</sub>/*n*. The asymmetric unit consists of one Co(II) ion, one fully protonated H<sub>2</sub>TPAA ligand, two HTPAA<sup>−</sup> anions (denoted as L<sub>As11</sub>, L<sub>As21</sub> and L<sub>As31</sub>) and one lattice water molecule (ESI, Fig. S1a). The Co(II) ion adopts an octahedral coordination geometry and its coordination sites are occupied by three nitrogen (N11<sup>ii</sup>, N21<sup>iii</sup> and N31) and three oxygen atoms (O11, O21 and O31<sup>i</sup>) that derive from six different ligands. The Co–O and Co–N bond lengths are in the range of 2.074(19)–2.1152(18) Å and 2.137(2)–2.181(2) Å, respectively, and are comparable to those of reported Co(II) phosphonates.<sup>19</sup> The As–O bonds are in a range of 1.6543(19)–1.729(2) Å (the above quoted bond lengths do not include the disordered arsonate functionality with lower site occupancy). The longer As–O bonds in the respective AsO<sub>3</sub> groups are As1A–O13 1.729 (2), As21–O23 1.699 (2) and As31–O33 1.726(2) Å, thus O13, O23 and O33 were assigned as hydroxyl moieties of protonated arsonate functionalities. Considering the charge balance of **1**, and the fact that the As21–O22 (1.684(2) Å) bond is longer than the As21–O21 (1.6543 (19) Å) bond, O22 was also assigned as a hydroxyl oxygen atom. The three different ligands all adopt the same ( $\kappa$ O- $\kappa$ N)- $\mu$  coordination mode (Fig. 1a). L<sub>As11</sub> and L<sub>As21</sub> link the Co(II) ions into a 1-D coordination assembly (Fig. 1b) which extends in the direction of the crystallographic *a*-axis, and which is further linked by L<sub>As31</sub> to form a 2-D network (Fig. 1c) that aligns parallel to the *ab*-plane. The closest distances between the neighboring Co(II) ions within this layer structure are 11.0190(21) Å (bridged by L<sub>As11</sub> and L<sub>As21</sub>) and 12.676(3) Å (bridged by L<sub>As31</sub>). Strong  $\pi \cdots \pi$  interactions prevail within the 1-D arrangement along the *a*-axis with centroidal distances between the phenyl and the triazole ring being 3.6405(7) and 3.6591(8) Å (Fig. 1b). There are two distinct, strong hydrogen-bond interactions in **1** that occur within the 2-D network between OH functionalities (O13 and O33) of the AsO<sub>3</sub> groups and deprotonated oxygen atoms (O31 and O21) of neighbouring AsO<sub>3</sub> groups. These H-bonds are characterised by O13–H13<sup>iii</sup>⋯O31<sup>i</sup> and O33–H33<sup>iii</sup>⋯O21<sup>iv</sup> distances of 2.659(3) and 2.771(3) Å, respectively [symmetry codes: (i) *x*, *y*−1, *z*; (iv) *x*, *y*+1, *z*]. Stronger intermolecular hydrogen-bond interactions also occur in a similar fashion between O23–H23<sup>iii</sup>⋯O32<sup>v</sup> of adjacent layers to give an O–O distance of 2.473(3) Å [symmetry codes: (v) −*x*+3/2, *y*−1/2, −*z*+1/2] (ESI, Fig. S1b). To the best of our knowledge, no organoarsionate-stabilised cobalt(II) coordination polymer has previously been reported.



(a)



(b)

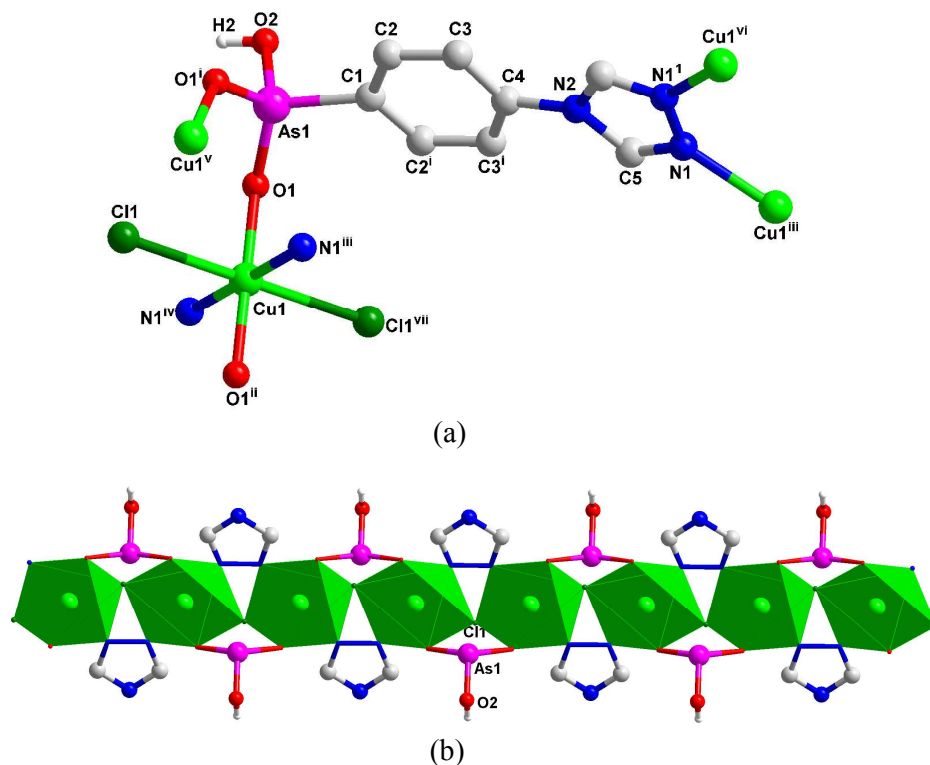


(c)

Fig. 1 (a) The coordination environment of Co(II) ion and the coordination modes of the ligands in **1**. Symmetry codes: (i)  $x, y-1, z$ ; (ii)  $x+1, y, z$ ; (iii)  $x-1, y, z$ ; (iv)  $x, y+1, z$ . (b) Polyhedral representation of the 1-D substructure in **1** comprising Co(II) ions and  $L_{As11}$ ,  $L_{As21}$  ligands (view in the direction of the crystallographic  $c$ -axis). (c) Polyhedral representation of the 2-D structure in **1** (view in the direction of the crystallographic  $c$ -axis).

**M(HTPAA)Cl·2H<sub>2</sub>O** (M = Cu (**2**), Co (**3**)) Compounds **2** and **3** are isostructural, crystallising in the space group  $C2/m$  and adopting similar cell parameters (Table 1). Therefore, only the structure of **2** will be discussed in detail. The asymmetric unit of **2** contains a half-occupied atom position of a Cu(II) ion, a HTPAA<sup>-</sup> anion, a Cl<sup>-</sup> and half-occupied atom positions of two lattice water molecules (ESI, Fig. S2a). In **2**, the Cu1 atom locates on an inversion centre, the Cl1 atom lies on a mirror plane and the HTPAA<sup>-</sup> ligand lies across a mirror plane with atom positions As1, O2, C1, C4, N2 located on the mirror plane. The Cu(II) ion has a slightly distorted octahedral coordination environment whose coordination sites are occupied by two nitrogen atoms (N1<sup>iii</sup> and N1<sup>iv</sup>), two oxygen atoms (O1 and O1<sup>ii</sup>) that derive from four different HTPAA<sup>-</sup> anions and two chlorine atoms (Cl1 and Cl1<sup>vii</sup>). The Cu1–O1 and Cu1–N1<sup>iii</sup> bond lengths range between 1.991(5) and 2.055(6) Å, respectively whilst the Cu1–Cl1 bond is 2.6801(18) Å long. The lengths of these Cu–O, Cu–N and Cu–Cl bonds in **2** are similar with reported values of comparable copper phosphonates.<sup>20</sup> The longest As–O bond of the As1O<sub>3</sub> functionality is As1–O2 (1.691(7) Å), and thus O2 was assigned as a hydroxyl oxygen atom. The HTPAA<sup>-</sup> anion adopts a ( $\kappa$ O, O'- $\kappa$ N, N')- $\mu_4$  coordination mode (Fig. 2a). The As1O<sub>3</sub> group and  $\mu$ -bridging Cl<sup>-</sup> anions link the Cu(II) ions into an 1-D substructure (Fig. 2b), which is further crosslinked by HTPAA<sup>-</sup> anions to form an 2-D coordination network that extends parallel to the crystallographic  $ab$  plane. The distance of adjacent Cu(II) ions within the 1-D assembly is 3.8576(8) Å; the closest distance between Cu(II) ions of adjacent chains is 10.227(2) Å. Strong intramolecular  $\pi \cdots \pi$  interactions exist within the layer. The centroidal distance between the phenyl and the triazole ring is 3.5112(12) Å (Fig. 2c). Strong intramolecular hydrogen-bond interactions occur within this 2-D structure and prevail between the hydroxyl functionality of a AsO<sub>3</sub> group (O2) and one of the lattice water molecules (O4W) to give a O2–H2 $\cdots$ O4W distance of 2.661(12) Å. Two distinct intermolecular hydrogen-bond interactions occur between the

adjacent layers; these involve the lattice water molecules as well as the deprotonated arsonate functionality (O1) to give characteristic distances of  $O4W \cdots O3W^{iv}$  and  $O4W \cdots O1^{viii}$  of 2.845(11) and 2.8394(65) Å, respectively [symmetry codes: (iv)  $x+1/2, y-1/2, z$ ; (viii)  $-x+3/2, y-1/2, -z$ ]. Furthermore, parallel aligned layers stack in the direction of the crystallographic  $c$ -axis in an AA fashion to form a 3-D supramolecular architecture through hydrogen-bonds involving the H-bond donor/acceptor pairs  $O2-H2 \cdots O4W$  and  $O4W \cdots O1^{viii}$  (ESI, Fig. S2b). A search in the Cambridge Crystallographic Database, CCDC, underlines the novelty of the here presented structure as only a few copper(II) arsonate coordination polymers that are stabilised by *o*-sulfophenylarsonate have previously been reported.<sup>11d</sup>



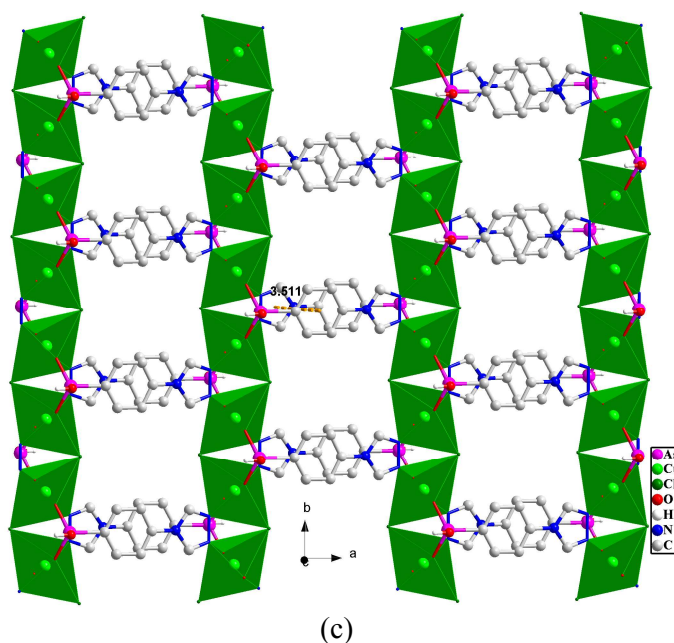
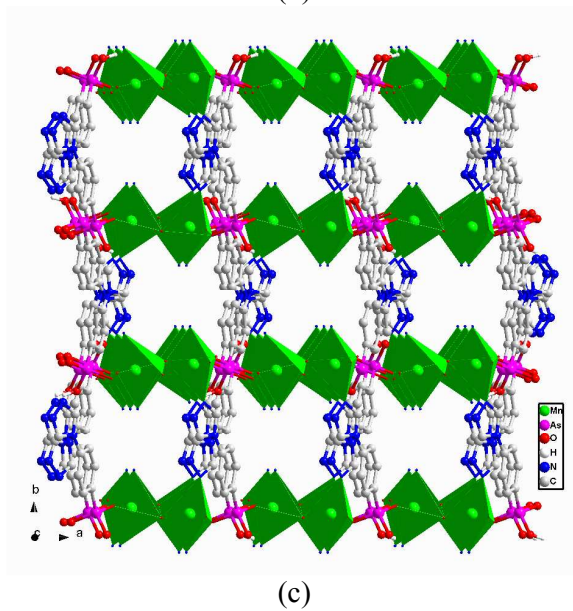
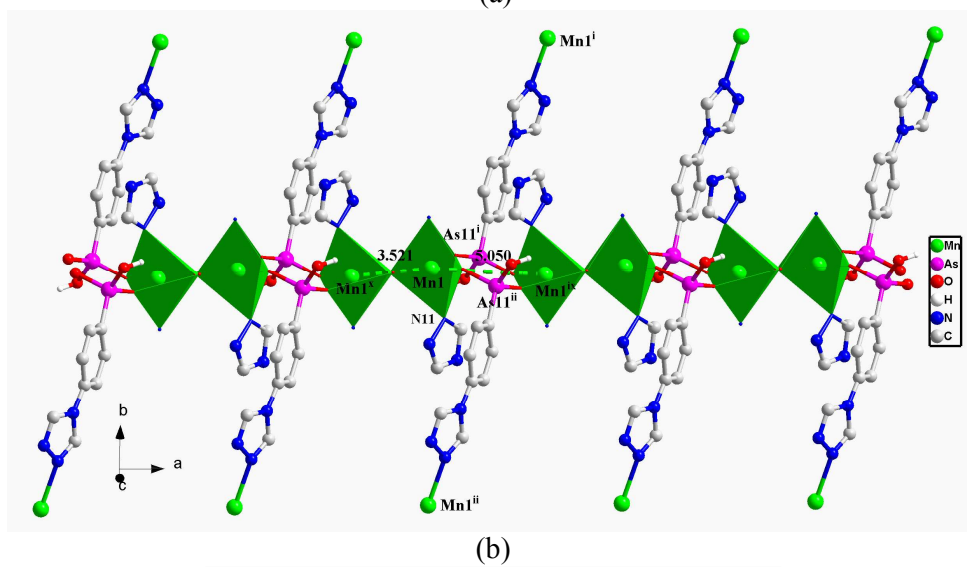
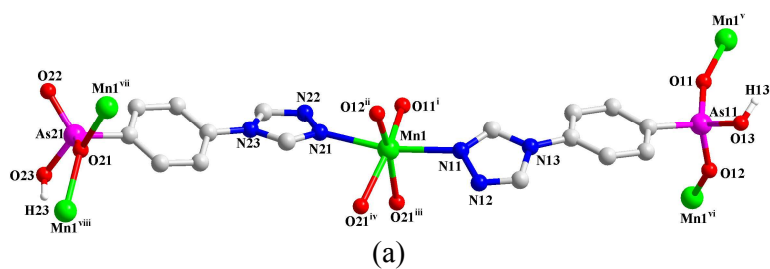
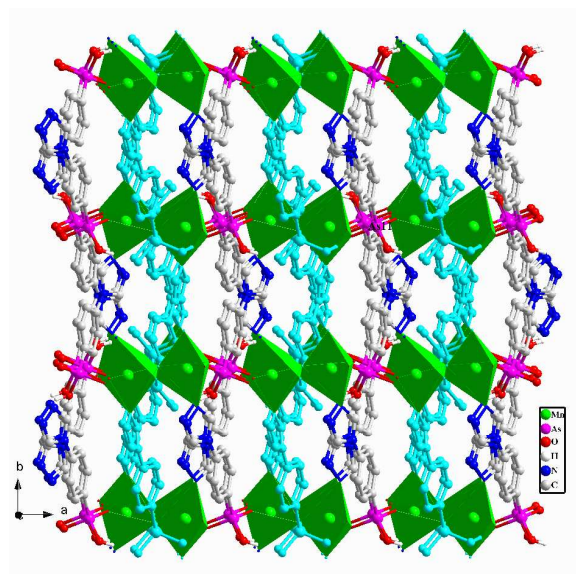


Fig. 2 (a) The coordination environment of the Cu(II) ion and the coordination mode of the ligand in **2**. Symmetry codes: (i)  $x, -y, z$ ; (ii)  $-x+3/2, -y+1/2, -z+1$ ; (iii)  $-x+1, y, -z+1$ ; (iv)  $x+1/2, -y+1/2, z$ ; (v)  $-x+3/2, y-1/2, -z+1$ ; (vi)  $x-1/2, y-1/2, z$ ; (vii)  $-x+3/2, y+1/2, -z+1$ . (b) Polyhedral representation of the 1-D substructure along the  $b$ -axis in **2** involving Cu(II) and, Cl<sup>-</sup> and the As1O<sub>3</sub> moiety. (c) Polyhedral representation of the 2-D structure in **2** (view in the direction of the crystallographic  $c$ -axis).

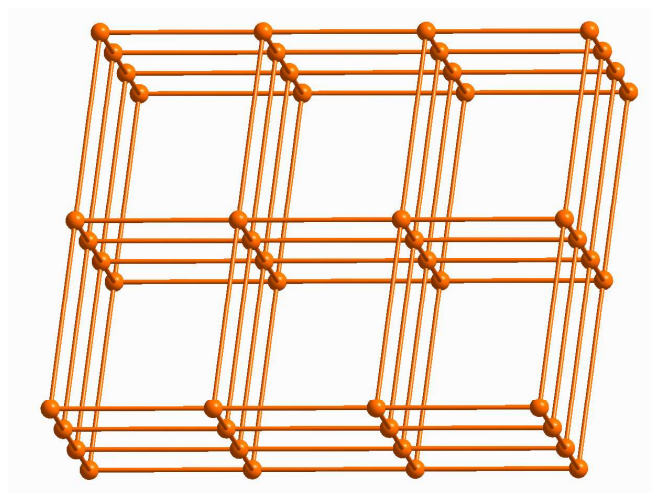
**M(HTPAA)<sub>2</sub>** (**M** = Mn, **4**; **M** = Cd, **5**) Compounds **4** and **5** are isostructural and herein we only depict the structural details for **4**. Single crystal X-ray diffraction studies reveal that the asymmetric unit of **4** consists of one Mn(II) ion and two HTPAA<sup>-</sup> anions (denoted as L<sub>As11</sub> and L<sub>As21</sub>) (ESI, Fig. S4a). The Mn(II) ion adopts a distorted octahedral coordination geometry whose coordination sites are occupied by two nitrogen atoms (N11 and N21) and four oxygen atoms (O11<sup>i</sup>, O21<sup>ii</sup>, O21<sup>iii</sup> and O21<sup>iv</sup>) that altogether derive from six different organic ligands. The Mn–O (2.090(2)–2.255(2) Å) and Mn–N (2.279(2)–2.335(2) Å) distances are comparable to those of structurally related Mn<sup>II</sup> phosphonates.<sup>21</sup> The atoms O13 and O23 were assigned as hydroxyl oxygen atoms as the As11–O13 (1.7217(19) Å) and As21–O23 (1.7306(19) Å) bonds represent the longest As–O bonds in their respective AsO<sub>3</sub> groups. L<sub>As11</sub> and L<sub>As21</sub> adopt ( $\kappa$ O, O'- $\kappa$ N)- $\mu_3$  and ( $\kappa$ O, O- $\kappa$ N)- $\mu_3$  coordination modes, respectively (Fig. 3a). O21 of L<sub>As21</sub> and its symmetry equivalent bridge between two Mn centres to form dinuclear subunits in which the two distorted {Mn1O<sub>4</sub>N<sub>2</sub>} octahedra share a







(d)



(e)

Fig. 3 (a) The coordination environment of the Mn(II) ion and the coordination modes of the ligands in **4**. (b) Polyhedral representation of 1-D substructure in **4** whereby Mn(II) ions are linked through arsonate functionalities. Symmetry codes: (i)  $-x+1, y-1/2, -z+1/2$ ; (ii)  $x, -y+3/2, z+1/2$ ; (iii)  $x, -y+1/2, z-1/2$ ; (iv)  $-x, y+1/2, -z+3/2$ ; (v)  $-x+1, y+1/2, -z+1/2$ ; (vi)  $x, -y+3/2, z-1/2$ ; (vii)  $x, -y+1/2, z+1/2$ ; (viii)  $-x, y-1/2, -z+3/2$ . (ix)  $-x+1, -y+1, -z+2$ ; (x)  $-x, -y+1, -z+2$ . (c) Polyhedral representation of the 3-D structure in **4** highlighting the connectivity involving Mn(II) ions and  $L_{As11}$  ligands (view in the direction of the crystallographic  $c$ -axis). (d) Polyhedral representation of the 3-D structure in **4**. The  $L_{As21}$  ligands are highlighted as pale blue (view in the direction of the crystallographic  $c$ -axis). (e) The equivalent 3-D topological network of **4**.

### 3.2 X-ray powder, spectral and thermogravimetric analyses

The phase-purity of the here presented compounds was confirmed by powder X-ray diffraction (PXRD). The  $2\theta$  values of the major reflections of the experimentally recorded PXRD patterns of the bulk solids of **1–5** match well to those of the simulated patterns which were obtained from respective single-crystal data (ESI, Fig. S5a-e). The FT-IR spectra of the five compounds and H<sub>2</sub>TPAA show typical As–C stretching vibration bands at 1103 cm<sup>-1</sup> for **1**, 1110 cm<sup>-1</sup> for **2**, 1107 cm<sup>-1</sup> for **3**, 1099 cm<sup>-1</sup> for **4**, 1100 cm<sup>-1</sup> for **5** and 1103 cm<sup>-1</sup> for H<sub>2</sub>TPAA. The vibrations associated with the AsO<sub>3</sub> moiety are very strong and occur at 859 and 825 cm<sup>-1</sup> for **1**, 846 and 832 cm<sup>-1</sup> for **2**, 853 and 829 cm<sup>-1</sup> for **3**, 806 cm<sup>-1</sup> for **4**, 814 cm<sup>-1</sup> for **5** and 825 cm<sup>-1</sup> for H<sub>2</sub>TPAA (ESI, Fig. S6a-f).<sup>13</sup> The solid-state luminescent properties of H<sub>2</sub>TPAA and **5** were investigated at room temperature. For H<sub>2</sub>TPAA, an emission band maximum centered at 456 nm can be observed upon photoexcitation at 373 nm (ESI, Fig. S7). Compound **5** exhibits a similar emission band to that of the pure ligand H<sub>2</sub>TPAA centering at 452 nm upon photoexcitation at 373 nm (Fig. 4). Therefore, the fluorescent emission at 452 nm in **5** can be attributed to intraligand ( $\pi$ – $\pi^*$ ) fluorescence. The thermal stability of **1–5** was also examined by thermogravimetric analysis (TGA) in an air atmosphere between 30 and 800 °C (ESI, Fig. S8). The TGA curve of **1** reveals the removal of constitutional lattice water molecules between 30 to 280 °C. Complex **1** is stable up to 340 °C, after which the framework collapses due to the total oxidation of the organic ligand. **2** and **3** lose their respective lattice water molecules between 30 to 120 °C and 165 °C, whilst the oxidation of the organoarsenate ligands occurs above 240 °C. **4** and **5** are stable up to *ca.* 320 °C, after which, their frameworks decompose due to the oxidation of the ligands.

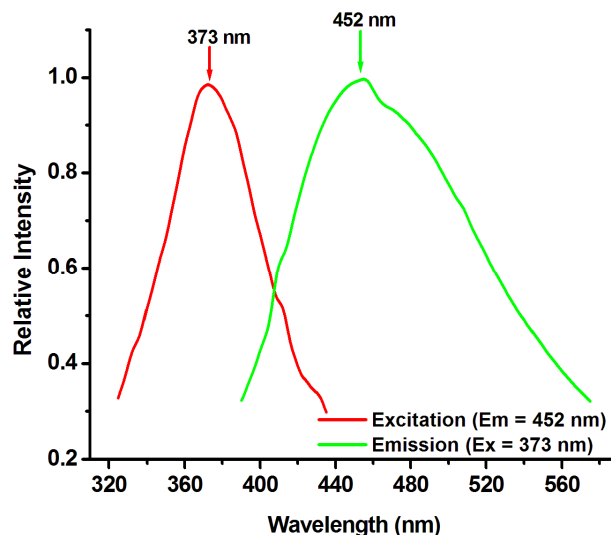


Fig. 4 Solid-state photoluminescent spectra of **5** measured at room temperature.

### 3.3 Magnetic properties of **2**, **3** and **4**

Magnetic susceptibility measurements of compounds **2** and **4** were performed as a function of the temperature in an applied dc field of 1 T. The temperature dependence of the  $\chi T$  product per  $\text{Cu}^{\text{II}}$  ion for **2** and per  $\text{Mn}^{\text{II}}$  ion for **4** are shown in Fig. 5 and Fig. 6, respectively. For **2**, the  $\chi T$  value at 300 K is  $0.41 \text{ cm}^3 \text{ K mol}^{-1}$  in good agreement with one isolated  $S = \frac{1}{2}$   $\text{Cu}^{\text{II}}$  ions and  $g = 2.1$ , while for **4**, the  $\chi T$  product at 300 K reaches  $4.1 \text{ cm}^3 \text{ K mol}^{-1}$  as expected for a high-spin  $S = 5/2$   $\text{Mn}^{\text{II}}$  ion (with  $g = 1.94$ ). Upon cooling, the  $\chi T$  product decreases continuously, and reaches the value of  $0.04 \text{ cm}^3 \text{ K mol}^{-1}$  at 4.2 K for **2** and  $1.6 \text{ cm}^3 \text{ K mol}^{-1}$  at 2.8 K for **4**. This type of thermal behavior indicates predominant antiferromagnetic (AF) coupling between metal ions in both **2** and **4**. The predominant AF interactions are further confirmed by the negative Weiss constants  $\theta = -15 \text{ K}$  in **2** (between 50 and 300 K) and  $\theta = -2.7 \text{ K}$  in **4** (between 3 and 300 K) derived from the Curie–Weiss law. To determine the exchange parameter between adjacent  $\text{Cu}^{\text{II}}$  ions ( $J$ ) in **2**, the experimental  $\chi T$  data were fitted using a Heisenberg chain model of quantum spins as derived by Bonner and Fisher using the following Hamiltonian  $H = -2J\sum S_i S_{i+1}$ .<sup>22</sup> Employing the well-known Bonner-Fisher numerical expression of the susceptibility.<sup>21</sup> The experimental data were fitted over the entire temperature range with  $g = 2.16(5)$  and  $J/k_{\text{B}} = -13.8(2) \text{ K}$  (see solid red line in Fig. 5). The negative  $J$  value is consistent with significant antiferromagnetic interactions

along the chain (Fig. 2b) between  $\text{Cu}^{\text{II}}$  ions in **2** through the unprecedented  $\text{OAs1O}_2$  (arsonate) /  $\mu\text{-Cl}^-$  / N1N2 (triazol group) bridge.

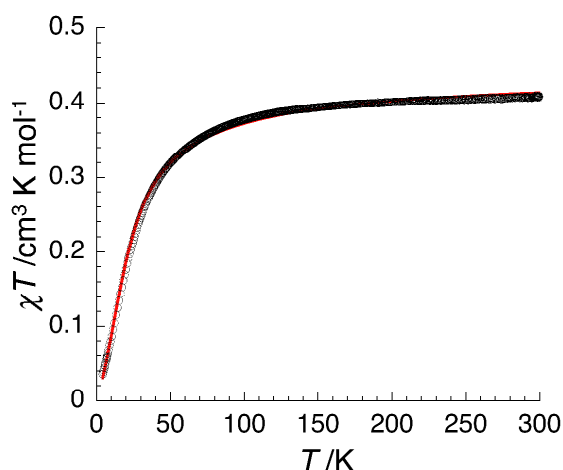


Fig. 5 Temperature dependence of the  $\chi T$  product for **2** at 1 T (with  $\chi$  defined as the molar magnetic susceptibility equal to  $M/H$  and normalized per  $\text{Cu}(\text{II})$  center). The solid red line indicates the best fit according to the  $S = 1/2$  chain model described in the text.

Considering the structure of **4**, two possible exchange pathways can be considered: exchange involving (i) the double  $\mu\text{-O}$  bridge within the dinuclear  $\text{Mn}(\text{II})$  units and (ii) the double *syn-syn* coordinating arsonate bridge (Fig. 3b). However, it is expected that the double  $\mu\text{-O}$  bridge promotes significantly stronger magnetic coupling than the arsonates. Thus the magnetic data were modeled using a Heisenberg  $S = 5/2$  spin-dimer model considering the following isotropic spin Hamiltonian  $H = -2JS_1S_2$ . According to this approach in the low field approximation, the magnetic susceptibility is given by:

$$\chi = \frac{Ng^2\mu_B^2}{k_B T} \times \frac{2\exp(2x) + 10\exp(6x) + 28\exp(12x) + 60\exp(20x) + 110\exp(30x)}{1 + 3\exp(2x) + 5\exp(6x) + 7\exp(12x) + 9\exp(20x) + 11\exp(30x)}$$

with  $x = J/(k_B T)$ . The experimental data are perfectly fitted by this analytical expression allowing the accurate determination of the magnetic parameters:  $g = 1.94(5)$  and  $J/k_B = -0.36(3)$  K. Hence, this model clearly demonstrates that the antiferromagnetic exchange interaction between the two magnetic centers within the dinuclear  $\text{Mn}(\text{II})$  moiety of **4** is rather weak. Nevertheless, this value is in agreement with the magnetic coupling observed in related  $\text{Mn}^{\text{II}}$  arsonate compounds, which possess also dinuclear double  $\mu\text{-O}$  bridged units.<sup>11d</sup>

On the other hand, the observed  $J$  value is smaller than corresponding  $J$  values of structurally related Mn(II) phosphonates.<sup>23</sup>

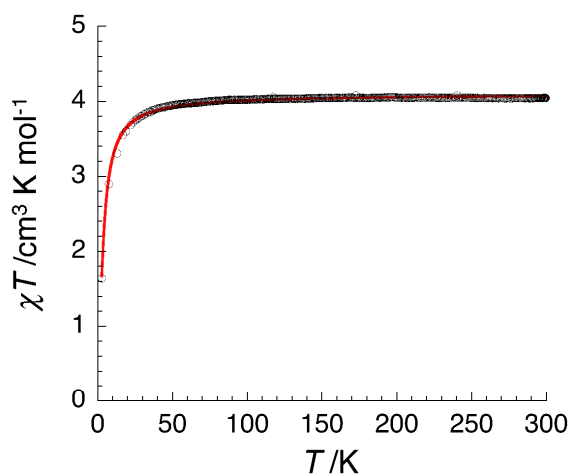


Fig. 6 Temperature dependence of the  $\chi T$  product for **4** at 1 T (with  $\chi$  defined as the molar magnetic susceptibility equal to  $M/H$  and normalized per Mn(II) center). The solid red line indicates the best fit according to the Heisenberg  $S = 5/2$  spin-dimer model described in the text.

The temperature-dependence of the  $\chi T$  product per Co<sup>II</sup> ion for **3** is shown in Fig. 7. The  $\chi T$  value at 300 K is  $3.1 \text{ cm}^3 \text{ K mol}^{-1}$  falls well within the expected range for octahedrally coordinated Co(II) ions. In this type of complex, the unquenched orbital momenta usually lead to relatively large  $g$  factors, in the present case of *ca.* 2.57 ( $S = 3/2$ ). Upon cooling, the  $\chi T$  product decreases slowly to a minimum of  $2.6 \text{ cm}^3 \text{ K mol}^{-1}$  at 22 K and then increases to a maximum of  $7.8 \text{ cm}^3 \text{ K mol}^{-1}$  at 1.8 K. The decrease of the  $\chi T$  product above 22 K may be caused by two effects: (i) the possible spin-orbit coupling of the Co(II) ions, and/or (ii) antiferromagnetic interactions between the Co(II) spin centres. Unfortunately for octahedral Co(II) systems, it is not possible to separate and/or discriminate between the two phenomena and thus it is extremely difficult to speculate on the nature of the magnetic interactions between Co(II) centers. Below 22 K, the increase of the  $\chi T$  product is also not conclusive as it could be the signature of ferromagnetic interactions between Co(II) sites along the chain (Fig. S3c) as well as non-compensating canted spins involving antiferromagnetic interactions along the chain (it is worth noting that two Co(II) orientations are present within the 1-D coordination polymer).

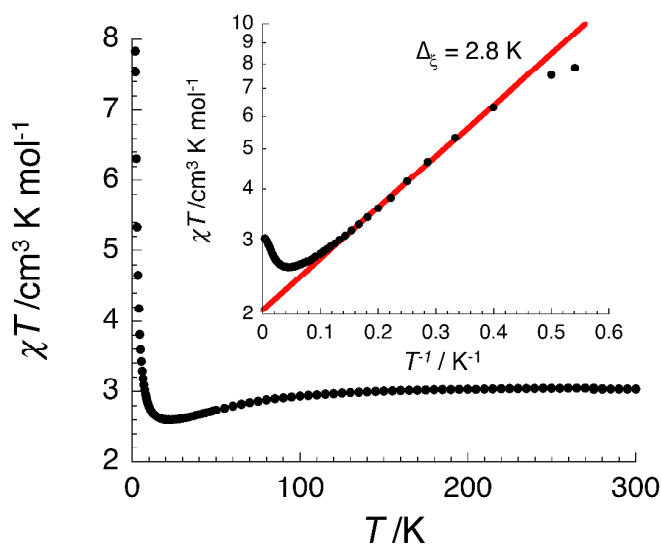


Fig. 7 Temperature dependence of the  $\chi T$  product for **3** at 1000 Oe (with  $\chi$  defined as the molar magnetic susceptibility equal to  $M/H$  and normalized per Co(II) center). Inset:  $\ln(\chi T)$  vs.  $1/T$  plot of **3**; the solid red line is the best exponential fit of the experimental data between 9 and 2.5 K.

The increase of the  $\chi T$  product below 22 K can be analysed in terms of correlation length ( $\xi$ ), as  $\xi$  is proportional to  $\chi T$  in any 1-D classical problem (in the low field limit). Moreover, for any one-dimensional spin system with uniaxial anisotropy (Ising or anisotropic Heisenberg spins), the correlation length diverges exponentially when the temperature is lowered according to  $\xi \propto \exp(\Delta_\xi/k_B T)$  and thus  $\chi T = C_{\text{eff}} \exp(\Delta_\xi/k_B T)$  (with  $\Delta_\xi$  being the energy to create a domain wall along the chain).<sup>24</sup> The dimensionality of the correlations is clearly one-dimensional based on the  $\ln(\chi T)$  vs  $1/T$  plot shown in inset of Fig. 7. It proves that the increase of the  $\chi T$  product below 10 K is produced by the interactions along the Co(II) chain shown in Fig. S3c. The correlation energy gap,  $\Delta_\xi$  of 2.8 K emphasizes the weak nature of the ferromagnetic interactions along the chain or indicates that the spins are strongly canted inducing a large compensation of the moments along the chain. As for the  $\chi T$  vs  $T$  data, the analysis of the correlation length does not allow one to decide which of the two scenario, i.e. ferromagnetic coupled spins or canted spins along the chain, takes preference. Finally, the field dependences of the magnetization measured at different temperatures were recorded below 8 K (Fig. 8 and Fig. S12). As seen in Fig. 8 and in its inset, the increase of the magnetization at low field is observed without any inflection point (i.e.  $S$  shape), in strong

support with the absence of antiferromagnetic interactions and thus suggesting the presence of ferromagnetic interactions along the chain between Co(II) magnetic sites.

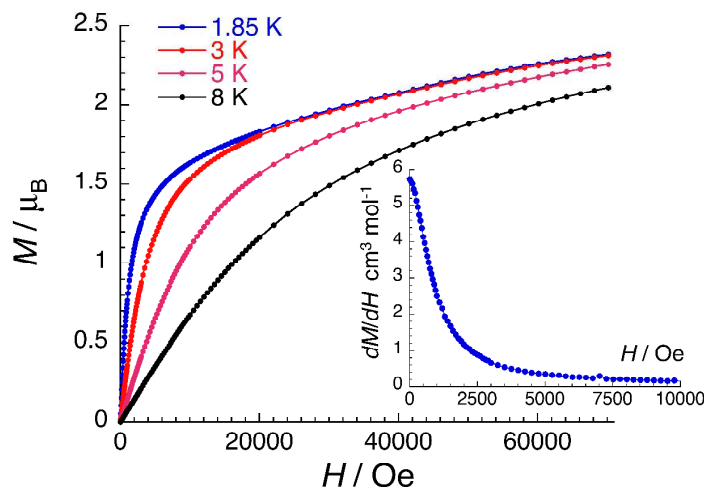


Fig. 8 Field dependence of the magnetization ( $M$ ) and, in inset, its field derivative ( $dM/dH$  at 1.8 K) for **4** at the temperatures indicated, scanning at 100 – 200 Oe·min<sup>-1</sup>.

At 1.8 K and 7 T, the magnetization reaches a value of 2.3  $\mu_B$  (Fig. 8) in good agreement with the values typically observed for a Co(II) ion.<sup>25</sup> Besides, the  $M$  versus  $H/T$  plots (Fig. S12) show a large deviation from scaling and are not super-imposable on a master curve indicating the presence of significant magnetic anisotropy in **3**, as it is expected for octahedral Co(II) metal ions.

From a magnetic point of view and based on the above analyses, compound **3** can be regarded a chain of ferromagnetically coupled anisotropic spins that thus contains all requirements to display Single-Chain Magnet behaviour.<sup>23</sup> Therefore, ac magnetic susceptibility measurements were performed in zero dc field between 1.8 and 15 K (Fig. S13) to probe slow dynamics of the magnetization in this compound. However, no out of phase signal was detected precluding (i) the presence of SCM properties in our experimental windows of temperature (above 1.8 K) and ac frequency (up to 1500 Hz) as well as (ii) the presence of a magnetic phase transition above 1.8 K.

#### 4 Conclusions

In summary, a new bifunctional arsonic acid ligand has been synthesized and its self-assembly in the presence of transition metal salts under hydrothermal condition has been investigated. Five new coordination polymers were isolated and their crystal structures,

luminescent and magnetic properties have been reported. As far as we know, **1** represents the first example of a Co(II) organoarsenate coordination polymer. Both **2** and **3** contain H<sub>2</sub>TPAA type ligands and coordinating chloride ions, which stabilise their respective 2-D structures. Compound **4** represents the first record of Mn(II) 3-D framework containing organoarsenate ligands. Our analyses of the magnetic properties of these arsonate-bridged coordination compounds provide rarely investigated insights into exchange pathways in this class of compound. Analyses of the magnetic properties reveal that **2** and **4** exhibit antiferromagnetic interactions between their respective magnetic centers; whilst **3** shows weak ferromagnetic interaction between the spin centers along its 1-D substructural network. Interestingly, **5** displays a typical ligand-centered fluorescence emission band. Our work shows that the arsonate functionality has a high propensity to be partially protonated under the applied reaction conditions. In this form, it has a lower tendency to bridge metal centers in comparison to the corresponding phosphonate ligands. All isolated coordination polymers contain partially deprotonated arsonic acid functionalities. This tendency can be interpreted in light of the p*K*<sub>a</sub> values. According to the literature, the p*K*<sub>a</sub> values of phenylphosphonic acid are 1.86 and 7.51,<sup>26</sup> and the p*K*<sub>a</sub> values of phenylarsonic acid are 3.8 and 8.5<sup>27</sup> suggesting that the 2<sup>nd</sup> deprotonation event occurs more readily for phosphonic acids than that for the arsonic acids. Despite the fact that arsonate anions can also adopt a variety of potential coordination modes, their ability as complexing agents has not yet been fully explored. Consequently, synthetic methodologies using organoarsenates require further investigations in order to fully understand the coordination chemistry of the resulting class of compound.

### Acknowledgements

We gratefully acknowledge the Science Foundation Ireland (SFI), the University of Bordeaux, the CNRS, the Aquitaine Région, and the ANR for financial support. Financial support from IRCSET (postdoctoral fellowship for Dr. Jian-Di Lin) is gratefully acknowledged.

### Reference

1. (a) J.-G. Mao, *Coord. Chem. Rev.*, 2007, **251**, 1493-1520; (b) E. Matczak-Jon and V. Videnova-Adrabińska, *Coord. Chem. Rev.*, 2005, **249**, 2458-2488; (c) H. L. Ngo and

- W. Lin, *J. Am. Chem. Soc.*, 2002, **124**, 14298-14299; (d) K. Maeda, *Microporous Mesoporous Mater.*, 2004, **73**, 47-55.
2. (a) A. K. Cheetham, G. Férey and T. Loiseau, *Angew. Chem., Int. Ed.*, 1999, **38**, 3268-3292; (b) C. N. R. Rao, S. Natarajan and R. Vaidhyanathan, *Angew. Chem., Int. Ed.*, 2004, **43**, 1466-1496; (c) T.-B. Liao, Y. Ling, Z.-X. Chen, Y.-M. Zhou and L.-H. Weng, *Chem. Commun.*, 2010, **46**, 1100-1102; (d) J.-T. Li, D.-K. Cao, T. Akutagawa and L.-M. Zheng, *Dalton Trans.*, 2010, **39**, 8606-8608; (e) J. Zhu, X. Bu, P. Feng and G. D. Stucky, *J. Am. Chem. Soc.*, 2000, **122**, 11563-11564.
3. (a) J.-T. Li, L.-R. Guo, Y. Shen and L.-M. Zheng, *CrystEngComm*, 2009, **11**, 1674-1678; (b) J.-T. Li, D.-K. Cao, B. Liu, Y.-Z. Li and L.-M. Zheng, *Cryst. Growth Des.*, 2008, **8**, 2950-2953; (c) S.-S. Bao, L.-F. Ma, Y. Wang, L. Fang, C.-J. Zhu, Y.-Z. Li and L.-M. Zheng, *Chem.–Eur. J.*, 2007, **13**, 2333-2343; (d) J. M. Taylor, R. K. Mah, I. L. Moudrakovski, C. I. Ratcliffe, R. Vaidhyanathan and G. K. H. Shimizu, *J. Am. Chem. Soc.*, 2010, **132**, 14055-14057; (e) S. R. Miller, G. M. Pearce, P. A. Wright, F. Bonino, S. Chavan, S. Bordiga, I. Margiolaki, N. Guillou, G. r. Férey, S. Bourrelly and P. L. Llewellyn, *J. Am. Chem. Soc.*, 2008, **130**, 15967-15981; (f) J.-L. Song and J.-G. Mao, *Chem.–Eur. J.*, 2005, **11**, 1417-1424; (g) C. Serre, J. A. Groves, P. Lightfoot, A. M. Z. Slawin, P. A. Wright, N. Stock, T. Bein, M. Haouas, F. Taulelle and G. Férey, *Chem. Mater.*, 2006, **18**, 1451-1457; (h) E. Burkholder, V. Golub, C. J. O'Connor and J. Zubieta, *Inorg. Chem.*, 2004, **43**, 7014-7029.
4. (a) S. Konar and A. Clearfield, *Inorg. Chem.*, 2008, **47**, 5573-5579; (b) M. Shanmugam, G. Chastanet, T. Mallah, R. Sessoli, S. J. Teat, G. A. Timco and R. E. P. Winpenny, *Chem.–Eur. J.*, 2006, **12**, 8777-8785; (c) V. Kubiček, J. Kotek, P. Hermann and I. Lukeš, *Eur. J. Inorg. Chem.*, 2007, **2007**, 333-344; (d) S. Konar, J. Zoň, A. V. Prosvirin, K. R. Dunbar and A. Clearfield, *Inorg. Chem.*, 2007, **46**, 5229-5236; (e) S.-F. Tang, J.-L. Song, X.-L. Li and J.-G. Mao, *Cryst. Growth Des.*, 2006, **7**, 360-366.
5. (a) F. Zhai, Q. Zheng, Z. Chen, Y. Ling, X. Liu, L. Weng and Y. Zhou, *CrystEngComm*, 2013, **15**, 2040-2043; (b) F. Zhai, M. Deng, Y. Ling, Z. Chen, L. Weng and Y. Zhou, *Inorg. Chim. Acta*, 2013, **402**, 104-108.
6. (a) E. Burkholder and J. Zubieta, *Inorg. Chim. Acta*, 2004, **357**, 301-304; (b) Y.-D. Chang and J. Zubieta, *Inorg. Chim. Acta*, 1996, **245**, 177-198; (c) L. Ben-Yao, K.

- Yih-Tong and W. Xin, *Inorg. Chim. Acta*, 1989, **161**, 233-237; (d) E. Burkholder, S. Wright, V. Golub, C. J. O'Connor and J. Zubieta, *Inorg. Chem.*, 2003, **42**, 7460-7471; (e) K. M. Barkigia, L. M. Rajkovic-Blazer, M. T. Pope and C. O. Quicksall, *Inorg. Chem.*, 1981, **20**, 3318-3323; (f) B. Liu, Y. Ku, M. Wang and P. Zheng, *Inorg. Chem.*, 1988, **27**, 3868-3871; (g) B. J. S. Johnson, R. C. Schroden, C. Zhu, V. G. Young and A. Stein, *Inorg. Chem.*, 2002, **41**, 2213-2218; (h) W. Kwak, L. M. Rajkovic, J. K. Stalick, M. T. Pope and C. O. Quicksall, *Inorg. Chem.*, 1976, **15**, 2778-2783; (i) B. J. S. Johnson, R. C. Schroden, C. Zhu and A. Stein, *Inorg. Chem.*, 2001, **40**, 5972-5978; (j) B. J. S. Johnson, S. A. Geers, W. W. Brennessel, J. V. G. Young and A. Stein, *Dalton Trans.*, 2003, 4678-4681; (k) K. Y. Matsumoto, *Bull. Chem. Soc. Jpn.*, 1978, **51**, 492-498; (l) B.-Y. Liu, G.-Y. Xie, Y.-T. Ku and X. Wang, *Polyhedron*, 1990, **9**, 2023-2028; (m) M. I. Khan and J. Zubieta, *Angew. Chem., Int. Ed.*, 1994, **33**, 760-762; (n) M. I. Khan, Y. Chang, Q. Chen, H. Hope, S. Parking, D. P. Goshorn and J. Zubieta, *Angew. Chem., Int. Ed.*, 1992, **31**, 1197-1200; (o) C. I. Onet, L. Zhang, R. Clérac, J. B. Jean-Denis, M. Feeney, T. McCabe and W. Schmitt, *Inorg. Chem.*, 2010, **50**, 604-613.
7. (a) J. M. Breen, L. Zhang, R. Clement and W. Schmitt, *Inorg. Chem.*, 2011, **51**, 19-21; (b) J. M. Breen, R. Clerac, L. Zhang, S. M. Cloonan, E. Kennedy, M. Feeney, T. McCabe, D. C. Williams and W. Schmitt, *Dalton Trans.*, 2012, **41**, 2918-2926; (c) J. M. Breen and W. Schmitt, *Angew. Chem., Int. Ed.*, 2008, **47**, 6904-6908; (d) L. Zhang and W. Schmitt, *J. Am. Chem. Soc.*, 2011, **133**, 11240-11248.
8. Y.-P. Xie, J. Yang, J.-F. Ma, L.-P. Zhang, S.-Y. Song and Z.-M. Su, *Chem.–Eur. J.*, 2008, **14**, 4093-4103.
9. (a) N. V. Izarova, M. H. Dickman, R. N. Biboum, B. Keita, L. Nadjo, V. Ramachandran, N. S. Dalal and U. Kortz, *Inorg. Chem.*, 2009, **48**, 7504-7506; (b) M. Barsukova, N. V. Izarova, R. N. Biboum, B. Keita, L. Nadjo, V. Ramachandran, N. S. Dalal, N. S. Antonova, J. J. Carbó, J. M. Poblet and U. Kortz, *Chem.–Eur. J.*, 2010, **16**, 9076-9085.
10. T. Tian, W. Yang, Q.-J. Pan and Z.-M. Sun, *Inorg. Chem.*, 2012, **51**, 11150-11154.
11. (a) T.-H. Zhou, J. Zhang, H.-X. Zhang, R. Feng and J.-G. Mao, *Chem. Commun.*, 2011, **47**, 8862-8864; (b) F.-Y. Yi, H.-B. Xu, T.-H. Zhou and J.-G. Mao, *CrystEngComm*, 2011, **13**, 1480-1489; (c) F.-Y. Yi, N. Zhao, W. Wu and J.-G. Mao,

- Inorg. Chem.*, 2009, **48**, 628-637; (d) F.-Y. Yi, Q.-P. Lin, T.-H. Zhou and J.-G. Mao, *J. Mol. Struct.*, 2010, **984**, 416-423.
12. W.-Z. Lin, Z.-Q. Liu, X.-H. Huang, H.-H. Li, S.-T. Wu and C.-C. Huang, *Chinese J. Struct. Chem.*, 2012, **31**, 1301-1308.
13. Z.-Q. Liu, Y.-F. Zhao, X.-H. Huang, H.-H. Li and C.-C. Huang, *Chinese J. Struct. Chem.*, 2010, **29**, 1724-1730.
14. F.-Y. Yi, J.-L. Song, N. Zhao and J.-G. Mao, *J. Solid State Chem.*, 2008, **181**, 1393-1401.
15. X.-Y. Qian, J.-H. Zhang, T.-H. Zhou and J.-G. Mao, *Dalton Trans.*, 2012, **41**, 1229-1236.
16. A. D. Naik, J. Marchand-Brynaert and Y. Garcia, *Synthesis*, 2008, **2008**, 149-154.
17. O. V. Dolomanov, L. J. Bourhis, R. J. Gildea, J. A. K. Howard and H. Puschmann, *J. Appl. Cryst.*, 2009, **42**, 339-341.
18. G. M. Sheldrick, *Acta Cryst.*, 2007, **A64**, 112-122.
19. (a) J.-L. Song, Andrey V. Prosvirin, H.-H. Zhao and J.-G. Mao, *Eur. J. Inorg. Chem.*, 2004, **2004**, 3706-3711; (b) J.-L. Song, H.-H. Zhao, J.-G. Mao and K. R. Dunbar, *Chem. Mater.*, 2004, **16**, 1884-1889; (c) P.-F. Wang, Y. Duan, J. M. Clemente-Juan, Y. Song, K. Qian, S. Gao and L.-M. Zheng, *Chem.-Eur. J.*, 2011, **17**, 3579-3583.
20. (a) V. Chandrasekhar, T. Senapati, E. C. Sañudo and R. Clérac, *Inorg. Chem.*, 2009, **48**, 6192-6204; (b) V. Chandrasekhar, P. Sasikumar, T. Senapati and A. Dey, *Inorg. Chim. Acta*, 2010, **363**, 2920-2928; (c) K. J. Gagnon, A. V. Prosvirin, K. R. Dunbar, S. J. Teat and A. Clearfield, *Dalton Trans.*, 2012, **41**, 3995-4006.
21. (a) S.-S. Bao, G.-S. Chen, Y. Wang, Y.-Z. Li, L.-M. Zheng and Q.-H. Luo, *Inorg. Chem.*, 2006, **45**, 1124-1129; (b) C. A. Merrill and A. K. Cheetham, *Inorg. Chem.*, 2006, **46**, 278-284; (c) P. Yin, S. Gao, Z.-M. Wang, C.-H. Yan, L.-M. Zheng and Xin, *Inorg. Chem.*, 2005, **44**, 2761-2765.
22. M. E. Fisher, *Am. J. Phy.*, 1964, **32**, 343.
23. Z.-Y. Du, A. V. Prosvirin and J.-G. Mao, *Inorg. Chem.*, 2007, **46**, 9884-9894.
24. (a) C. Coulon, H. Miyasaka and R. Clérac, in *Single-Molecule Magnets and Related Phenomena*, ed. R. Winpenny, Springer Berlin Heidelberg, 2006, vol. 122, pp. 163-206; (b) H. Miyasaka, M. Julve, M. Yamashita and R. Clérac, *Inorg. Chem.*, 2009, **48**, 3420-3437; (c) X.-B. Li, G.-M. Zhuang, X. Wang, K. Wang and E.-Q. Gao, *Chem. Commun.*, 2013, **49**, 1814-1816.

25. (a) K. G. Alley, R. Bircher, O. Waldmann, S. T. Ochsenbein, H. U. Güdel, B. Moubaraki, K. S. Murray, F. Fernandez-Alonso, B. F. Abrahams and C. Boskovic, *Inorg. Chem.*, 2006, **45**, 8950-8957; (b) F. Klöwer, Y. Lan, J. Nehr Korn, O. Waldmann, C. E. Anson and A. K. Powell, *Chem.–Eur. J.*, 2009, **15**, 7413-7422.
26. K. Nagarajan, K. P. Shelly, R. R. Perkins and R. Stewart, *Can. J. Chem.*, 1987, **65**, 1729-1733.
27. S. Zheng, Y. Cai and K. E. O'Shea, *J. Photochem. Photobiol. A–Chem.*, 2010, **210**, 61-68.